

IEEE TRANSACTIONS ON CONTROL SYSTEMS TECHNOLOGY



A PUBLICATION OF THE IEEE CONTROL SYSTEMS SOCIETY

JULY 2009

VOLUME 17

NUMBER 4

IETTE2

(ISSN 1063-6536)

PAPERS

Predictive Guidance of a Projectile for Hit-to-Kill Interception	<i>P. V. Hahn, R. A. Frederick, and N. Slegers</i>	745
Incremental Step Reference Governor for Load Conditioning of Hybrid Fuel Cell and Gas Turbine Power Plants	<i>V. Tsourapas, J. Sun, and A. Stefanopoulou</i>	756
Adjusting Output-Limiter for Stable Haptic Rendering in Virtual Environments	<i>K. Lee and D. Y. Lee</i>	768
A Qualitative Event-Based Approach to Continuous Systems Diagnosis	<i>M. J. Daigle, X. D. Koutsoukos, and G. Biswas</i>	780
Multi-Objective Robust H_∞ Control of Spacecraft Rendezvous	<i>H. Gao, X. Yang, and P. Shi</i>	794
Adaptive Control of an Electrically Driven Nonholonomic Mobile Robot via Backstepping and Fuzzy Approach	<i>Z.-G. Hou, A.-M. Zou, L. Cheng, and M. Tan</i>	803
Nonlinear Control Design for a Supercavitating Vehicle	<i>X. Mao and Q. Wang</i>	816

BRIEF PAPERS

Decreasing the Apparent Inertia of an Impedance Haptic Device by Using Force Feedforward	<i>J. J. Gil, A. Rubio, and J. Savall</i>	833
A Note on Integer Programming Formulations of the Real-Time Optimal Scheduling and Flight Path Selection of UAVs ..	<i>B. Alidaee, H. Wang, and F. Landram</i>	839
Control of a 5DOF Magnetically Levitated Positioning Stage	<i>C. Fulford, M. Maggiore, and J. Apkarian</i>	844
Partial-Energy-Shaping Control for Orbital Stabilization of High-Frequency Oscillations of the Furuta Pendulum	<i>L. Freidovich, A. Shiriaev, F. Gordillo, F. Gómez-Estern, and J. Aracil</i>	853
Design of a Packet-Based Control Framework for Networked Control Systems	<i>Y.-B. Zhao, G.-P. Liu, and D. Rees</i>	859
An Optimal Control Method Based on the Energy Flow Equation	<i>N. Fukushima, M. S. Arslan, and I. Hagiwara</i>	866
Nonlinear Tracking Control of 3-D Overhead Cranes Against the Initial Swing Angle and the Variation of Payload Weight	<i>D. Chwa</i>	876

(Contents Continued on Back Cover)

To: Prof. Shuxiang Guo
Faculty of Eng.
University of Kagawa
Takamatsu
JAPAN

ICST/17/4/2014356



Celebrating 125 Years
of Engineering the Future

Singularity Avoidance of Control Moment Gyros by Predicted Singularity Robustness: Ground Experiment	884
..... <i>H. Leeghim, I.-H. Lee, D.-H. Lee, H. Bang, and J.-O. Park</i>	
Global Stability of a Saturated Nonlinear PID Controller for Robot Manipulators	892
..... <i>D. Sun, S. Hu, X. Shao, and C. Liu</i>	
Adaptive Control of Uncertain Hamiltonian Multi-Input Multi-Output Systems: With Application to Spacecraft Control ..	900
..... <i>H. Yoon and B. N. Agrawal</i>	
Modeling and Optimization Analysis of a Single-Flagellum Micro-Structure Through the Method of Regularized Stokeslets	907
..... <i>E. J. Lobaton and A. M. Bayen</i>	
Design of Minimal and Tolerant Sensor Networks for Observability of Vehicle Active Suspension	917
..... <i>A. Chamseddine, H. Noura, and M. Ouladsine</i>	
Design of Ternary Signals for MIMO Identification in the Presence of Noise and Nonlinear Distortion	926
..... <i>A. H. Tan, K. R. Godfrey, and H. A. Barker</i>	
Global Trajectory Tracking Through Static Feedback for Robot Manipulators With Bounded Inputs	934
..... <i>E. Aguiñaga-Ruiz, A. Zavala-Río, V. Santibáñez, and F. Reyes</i>	
Recursive Identification of Sandwich Systems With Dead Zone and Application	945
..... <i>Y. Tan, R. Dong, and R. Li</i>	
Modeling and Identification of Nonlinear Dynamics for Freeway Traffic by Using Information From a Mobile Cellular Network	952
..... <i>A. Alessandri, R. Bolla, M. Gaggero, and M. Repetto</i>	
Experimental Identification and Active Control of Configuration Dependent Linkage Vibration in a Planar Parallel Robot	960
..... <i>X. Wang, J. K. Mills, and S. Guo</i>	
Optimal Performance Tradeoffs in Repetitive Control: Experimental Validation on an Active Air Bearing Setup	970
..... <i>G. Pipeleers, B. Demeulenaere, F. Al-Bender, J. De Schutter, and J. Swevers</i>	
Path Generation and Tracking in 3-D for UAVs	980
..... <i>G. Ambrosino, M. Ariola, U. Ciniglio, F. Corraro, E. De Lellis, and A. Pironti</i>	

Experimental Identification and Active Control of Configuration Dependent Linkage Vibration in a Planar Parallel Robot

Xiaoyun Wang, *Member, IEEE*, James K. Mills, *Member, IEEE*, and Shuxiang Guo, *Senior Member, IEEE*

Abstract—In a lightweight planar parallel robot, unwanted linkage vibrations are induced during high-speed motion. The transfer functions from motor inputs to linkage vibrations are dependent on the robot configuration. In this work, we experimentally identify linkage vibrations by performing experimental modal analysis using lead zirconate titanate transducers. Then, the contributions of linkage modes are separated from configuration-dependent transfer functions. Through redefinition of vibration inputs, the flexible linkage dynamics is approximated by a linear dynamic model with variations of natural frequencies. Based on this simplification, a modal controller is designed to control two linkage modes. Experimental control results, yielding more than 50% reduction of vibration amplitudes of these two modes, validate the effectiveness of the proposed control strategy.

Index Terms—Active vibration control, experimental modal analysis (EMA), parallel robot, smart structures.

I. INTRODUCTION

SUPPRESSION of unwanted linkage vibrations caused by large inertial forces and external disturbances in lightweight mechanisms has attracted significant research interest. A variety of techniques, including optimization of linkage cross-section [1], utilization of high-performance composite materials [2], smart structure techniques [3], and passive damping materials [4], have been proposed to reduce the linkage vibrations.

Parallel mechanisms have recently been studied intensively because of their potential to achieve higher payload, higher speed, and higher accuracy than serial mechanisms [5]. A “smart parallel robot,” shown in Fig. 1 has been designed for high-speed manufacturing processes. The prismatic-revolute-revolute ($3\text{-}P\text{-}R\text{-}R$) kinematic architecture was selected based on an optimal effective workspace criterion [6]. To achieve high-speed motion, linkages are designed to be lightweight, however, vibrations may be induced due to inertial and driving forces. Due to their high force-output and fast dynamic response properties [3], piezoelectric ceramics are utilized to sense and control linkage vibrations.

For flexible-link robots with closed-loop architectures, the location of the end-effector cannot be expressed explicitly in

Manuscript received August 25, 2006; revised June 04, 2007. Manuscript received in final form May 05, 2008. First published May 05, 2009; current version published June 24, 2009. Recommended by Associate Editor M. de Mathelin.

X. Wang and J. K. Mills are with the Department of Mechanical and Industrial Engineering, University of Toronto, Toronto, ON M5S 3G8, Canada (e-mail: wangxia@aecl.ca; mills@mie.utoronto.ca).

S. Guo is with the Faculty of Engineering, Kagawa University, Takamatsu 150001, Japan, and also with Harbin Engineering University, Harbin 150001, China, and also with the University of Toronto, Toronto, ON M5S 3G8, Canada.

Color versions of one or more of the figures in this paper are available online at <http://ieeexplore.ieee.org>.

Digital Object Identifier 10.1109/TCST.2009.2014356

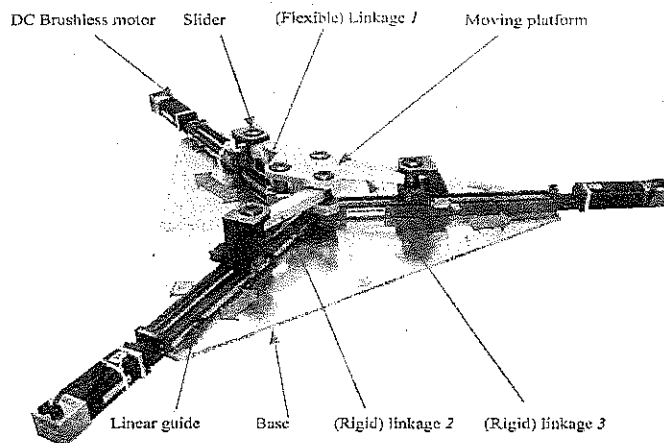


Fig. 1. Prototype of the “smart parallel robot”.

terms of actuated joint coordinates. The motion of multiple kinematic chains is coupled and the linkage vibration is nonlinearly coupled with rigid-body motion of the robot, and configuration dependent. Utilizing the moving-frame approach, a dynamic model of the parallel robot has been developed [7].

The main focus of this paper is to experimentally investigate the vibration characteristics of a single flexible linkage using lead zirconate titanate (PZT) transducers. Based on identification results in various configurations and operating conditions, an active vibration controller is designed and implemented to suppress linkage vibrations. Experimental results demonstrate the validity and robust behavior of this controller.

This paper is organized as follows. Section II reviews the relevant literature. Section III introduces the experimental setup used in this investigation. Section IV presents EMA results of one flexible linkage of the parallel robot. Based on assumptions made using EMA results, an active vibration controller is designed in Section V, with experimental results given. Finally, Section VI concludes this paper.

II. LITERATURE REVIEW

Work in [8]–[13] has been undertaken to introduce PZT materials for active vibration control of flexible mechanisms. Sung *et al.* [8], [9] investigated the usage of single PZT sensor and actuator to suppress linkage vibration of a four-bar linkage mechanism. Choi *et al.* [13] simulated linkage vibration control of a flexible mechanism using piezoelectric films.

The flexible mechanisms studied in the literature are either open loop mechanisms or with only one closed loop, such as a four-bar linkage or slider-crank mechanism. No experimental work has been reported addressing active vibration control of flexible mechanism with multiple kinematic chains. In these multi-chain mechanisms, the boundary conditions are not

simple and therefore must be identified. The coupling of rigid body motion and linkage vibrations also needs to be studied. Experimental modal analysis (EMA) [14], has been widely used in the experimental identification of structural dynamic behavior. Smart materials actuators and sensors are used to excite and sense structural vibration and may be further used to identify structural modal properties. Saunders *et al.* [15] derived an EMA formulation for a simply supported plate with PZT actuators and Polyvinylidene fluoride (PVDF) sensors. Wang *et al.* [16] discussed the feasibility of modal testing using PZT transducers using a cantilever beam.

Numerical studies demonstrate that vibration characteristics of flexible mechanisms typically exhibit both configuration-dependent and nonlinear properties [17]. Shabana [18] pointed out that development of experimental modal identification techniques for multi-body systems may be one of "the most challenging and interesting problems" in the analysis of multi-body systems. Hardage and Weins [19] used a hammer and an accelerometer to identify natural frequencies and damping ratios of a stationary parallel robot as a function of robot configuration. Wang and Mills generalized the modal identification procedure utilizing a combination of a number of transducers, including PZT transducers [20]. Since this paper is submitted, these authors further studied the control of vibrations in the linkages [21]. The work here investigates linkage vibration characteristics when the robot undergoes rigid body motion. Transfer functions from motor input to linkage vibration responses are simplified, which allows the proposed controller to be designed in modal domain.

III. EXPERIMENTAL SETUP

The experimental setup is introduced in this section. The experimental system is comprised of the parallel robot, a motion control system, active vibration control instruments, and a host computer with a MCX-DSP controller.

Fig. 2 shows a schematic of the parallel robot. The three prismatic joints, i.e., the three sliders shown in Fig. 2, are active joints, located at B_i , $i = 1, 2, 3$. Each prismatic joint is driven by a dc servo motor which actuates ball bearing lead screws. Each slider is connected to a linkage through a passive revolute joint at B_i , $i = 1, 2, 3$. Three linkages are connected to the moving platform with a passive revolute joint at C_i , $i = 1, 2, 3$. Linkage 1 is designed to be flexible to allow experimentation with vibration control, while the other two links are rigid. With dc motors, the moving platform of mass 4.049 kg, is positioned in the 40 cm \times 40 cm workspace, with a desired orientation. The platform can achieve a linear speed of 4 m/s, acceleration of 10g, and an accuracy of sub-10 μm [6].

In Fig. 2, a global coordinate system is shown as (x, y, φ) , with the origin located at the center of the workspace O . The position and orientation of the platform, at the mass center P , is defined as (x_p, y_p) and φ_p , respectively. Three active prismatic joints, i.e., sliders, moves along ball bearing lead screws, whose orientations are at angles α_i , measured with respect to the global x -axis, respectively, 270° , 30° , 150° . The origins of three ball bearing lead screws are indicated by A_i , $i = 1, 2, 3$. The coordinate from A_i to the location of the sliders B_i is defined as

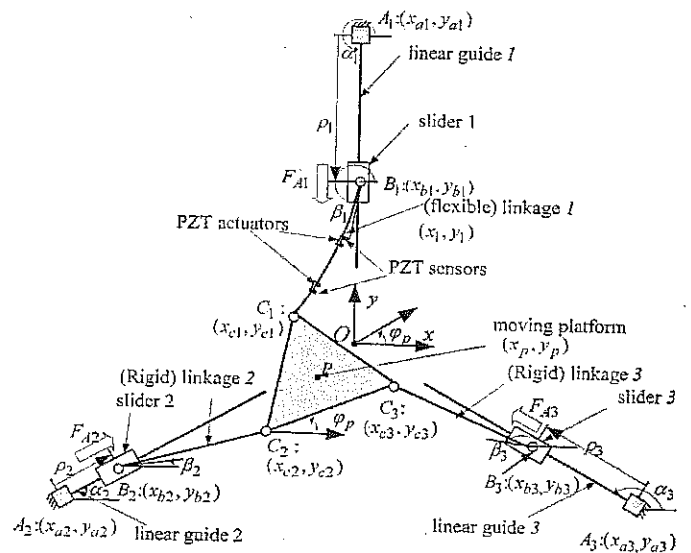


Fig. 2. Coordinate system of the planar parallel robot.

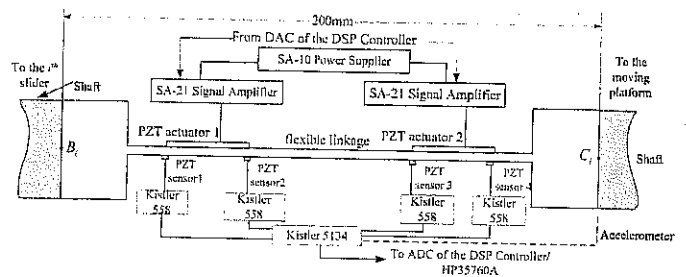


Fig. 3. Vibration control system for one flexible linkage.

ρ_i . The vector (ρ_1, ρ_2, ρ_3) denotes the robot configuration and $(0, 0, 0)$ is the home configuration.

Fig. 3 is a schematic of the active vibration control system for the flexible linkage, denoted as linkage 1 in Fig. 2. Four PZT sensors and two PZT actuators are bonded to this flexible linkage. The charge signals from the PZT sensors are converted to a voltage signal by impedance converters and then amplified by signal couplers. These amplified signals are sampled by the DSP unit which provides PZT drive signals which are filtered by second order Butterworth low pass filters.

IV. EXPERIMENTAL IDENTIFICATION OF THE MODAL PROPERTIES OF THE FLEXIBLE LINKAGE

The aim of this section is to identify the characteristics of linkage vibrations to be controlled, which occur when the robot undergoes rigid body motions. EMA is performed to characterize linkage vibrations with the robot in various configurations and operational conditions. Section IV-A introduces EMA results when the robot is stationary, i.e., when it can be considered as a linear structure. Section IV-B introduces linkage vibration responses when the robot undergoes rigid-body motions hence can no longer be considered as a linear structure. Section IV-C describes EMA of configuration-dependent frequency response functions (FRFs). Based on the EMA results, Section IV-D introduces simplifications of transfer functions from motor input

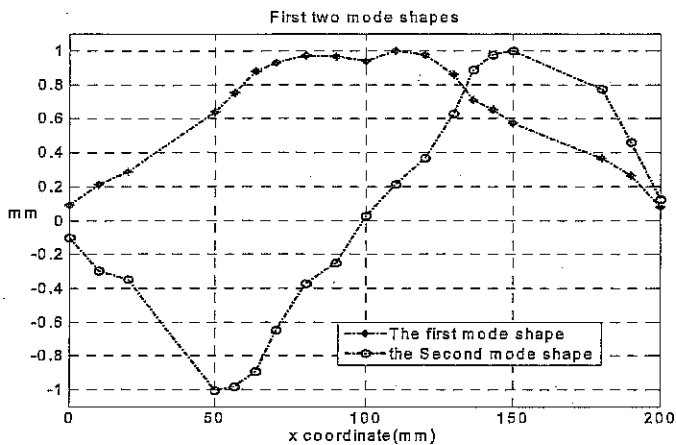


Fig. 4. First two mode shapes of the flexible linkage identified using an impact hammer and an accelerometer.

to linkage vibration responses. Section IV-E discusses the variation of natural frequencies for modes 1 and 4.

A. EMA of Linkage Vibration When the Robot is Stationary

EMA is a special case of system identification where an *a priori* model form consisting of modal parameters is assumed. Frequency domain methods extract modal properties from FRFs, which describes transfer properties of structures.

FRFs are acquired by dividing the Fourier transforms of responses by the Fourier transform of excitation signal [20]. According to analytical models, an FRF from an actuator at the k th degrees of freedom (DOF) to a sensor at the j th DOF has the following form [14]:

$$\alpha_{jk}(\omega) = \sum_{r=1}^N \frac{-\{\varphi_r\}_j \{\varphi_r\}_k}{m_r \left(\frac{\omega_r^2}{\omega^2 - 1} + \frac{2i\omega_r \xi_r}{\omega} \right)} + R_{I_{jk}} \quad (1)$$

where $m_r \triangleq r$ th modal mass, $\omega_r \triangleq r$ th natural frequency, $x \triangleq$ spatial coordinate for the linkage, $N \triangleq$ the number of modes, $\xi_r \triangleq$ damping ratio for the r th mode, $\varphi_r(x) \triangleq$ the r th mode shape, $R_{I_{jk}} \triangleq$ residual terms.

By performing modal tests on a series of FRFs modal shapes can be obtained. The form of FRF formulations and resultant modal shape vectors are dependent on the types of sensors and actuators used. In addition to FRFs using an impact hammer (with a load cell) and accelerometer combination, FRFs formulations for PZT sensors and actuators are given in [20].

Using four different types of FRFs, EMA is performed when the robot is stationary. These experiments give two most significant modes. Fig. 4 shows the mode shapes φ_r obtained using an impact hammer and an accelerometer, sequentially placed on the different locations x in (1) on the linkage to acquire different FRFs. The first and second mode at 94.14 and 323.71 Hz, respectively, are pinned-pinned modes. It is also observed that the natural frequencies of the linkages are dependent on configuration to a small extent. Here the variation is attributed to variations of constraints at the linkage boundaries at B_i and C_i in Fig. 2.

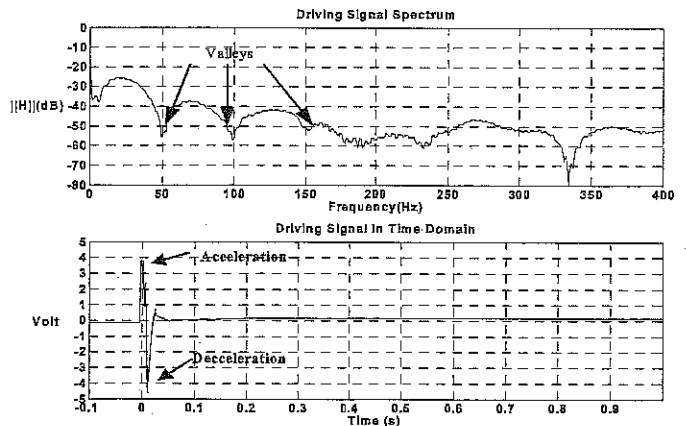


Fig. 5. Motor driving signal in frequency and time domain.

B. Linkage Vibrations During Rigid-Body Motion

Linkage vibration characteristics are examined when the robot undergoes rigid body motion starting from different configurations. During tests, slider 1 is set to have a displacement of 5 mm in 25 ms providing high acceleration to excite linkage modes, starting from different configurations. Driving signal is plotted in Fig. 5 in frequency and time domain.

Fig. 6 shows the acceleration spectrums at locations 1, 3, 5, and 7 when the robot moves 5 mm very rapidly starting from configurations $q^1 = (\rho_1, \rho_2, \rho_3) = (0, 0, 0)$ mm and $q^6 = (-50, 60, 10)$ mm. From Fig. 6, it is observed that frequency components of the response spectrums exhibit a large number of peaks. These multiple peaks arise because motion of the entire planar parallel robot is involved, including all the transmission components. As shown in Fig. 6, peak frequencies and amplitudes at peak frequencies vary with configuration, clearly demonstrating configuration-dependency vibrations.

C. Analysis of Configuration-Dependent FRFs

EMA is performed on the configuration dependent FRFs acquired at various configurations. As responses are configuration-dependent, FRFs are configuration-dependent as well. After analysis, the first four modes are determined and are plotted in Fig. 7 in three configurations q^1 , $q^3 = (60, 0, 0)$ mm, q^6 . The first and the fourth modes are basically the first two modes for a pinned-pinned beam. These two modes are essentially the same as obtained when the robot is stationary, as seen in Fig. 4. This shows that the mode shape vectors when the robot is stationary are a subset of those obtained during rigid body motion. The natural frequencies and mode shapes of these two pinned-pinned modes are close in different configurations although the amplitudes of FRFs are quite different at these frequencies.

In addition to two pinned-pinned modes, two other modes, i.e., mode 2 (between 140–160 Hz) and mode 3 (between 180–200 Hz) in Fig. 7, are also observed. The second mode resembles the first mode for a pinned-free beam: It is speculated that this mode is caused by the mobility of the moving platform, and is related to mechanical gaps in the robot joints. The third mode resembles the first mode for a free-pinned beam, which is confirmed to result from lateral flexibility of the lead screws.

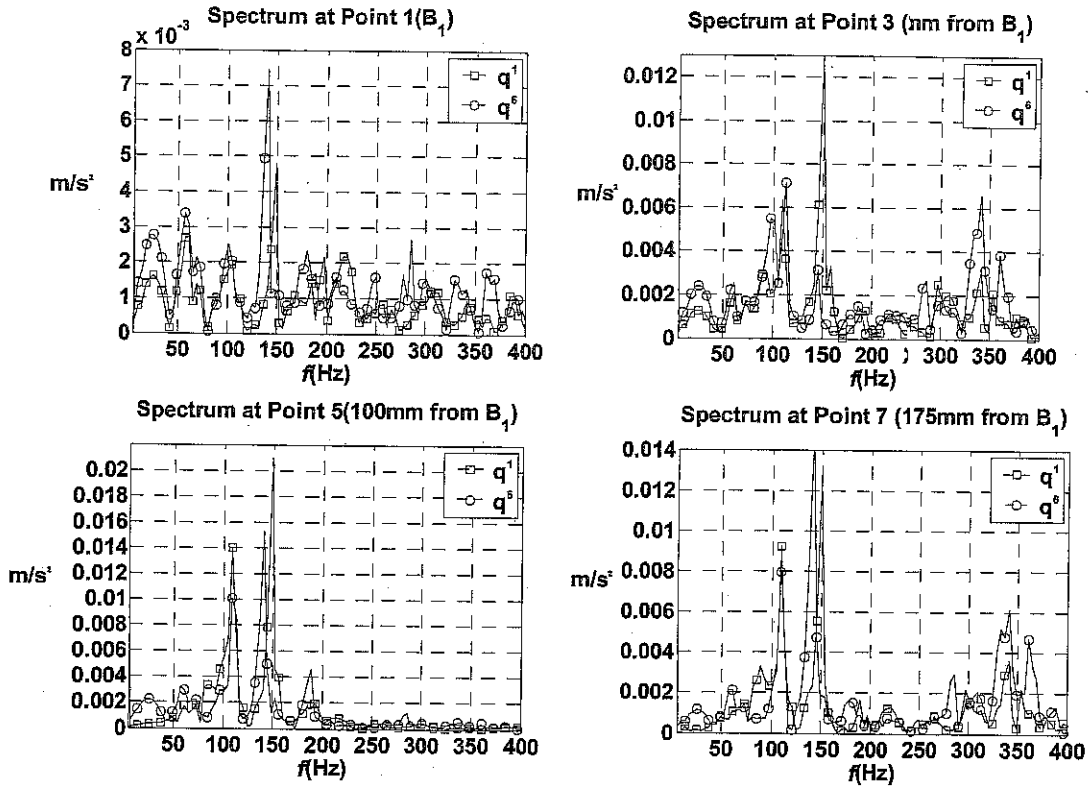


Fig. 6. Linkage acceleration spectrum during 5-mm translation of axis 1.

D. Simplification of Transfer Function From Motor Input to Linkage Vibration Responses

As discussed in Section IV-C, modes 2 and 3 are not mainly caused by linkage flexibility. Hence, the vibration for these two modes cannot be substantially reduced if only linkage vibration is controlled. The paper focuses on controlling linkage vibrations, hence only modes 1 and 4 are controlled.

Although FRFs from motor voltage input to linkage vibration response are configuration-dependent, it is observed that the changes in linkage mode shapes 1 and 4 are small. These frequencies also exhibit configuration-dependency to a limited degree. This configuration-dependency of FRFs amplitude and natural frequencies can be explained by a numerical dynamic model developed with the moving frame approach [7]. In the moving frame approach, flexible body dynamics is modeled using linear vibration theory in local frames. The coupling of flexible body deformation with rigid body motion is hence highly dependent on robot configuration as evidenced by the transformations from the local frames to the global frame, giving a configuration dependent inertia matrix.

In order to control two pinned-pinned modes, we separate the transfer function from motor voltage input to PZT sensor responses $\mathbf{G}(\mathbf{q}, s)$ into four parts: contributions of modes 2 and 3, i.e., $\mathbf{T}(\mathbf{q}, s)$, contributions from mode 1 and 4, i.e., $\mathbf{P}_1(s)$ and $\mathbf{P}_4(s)$, and residue error term $\Delta(\mathbf{q}, s)$

$$\mathbf{G}(\mathbf{q}, s) = \mathbf{T}(\mathbf{q}, s) + \mathbf{P}_1(\mathbf{q}, s) + \mathbf{P}_4(\mathbf{q}, s) + \Delta(\mathbf{q}, s) \quad (2)$$

where

$$\begin{aligned} \mathbf{T}(\mathbf{q}, s) &= \sum_{k=2,3} \frac{\mathbf{R}_k(\mathbf{q})}{s^2 + 2\xi_k \omega_k(\mathbf{q})s + \omega_k^2(\mathbf{q})} \\ &\triangleq \text{contribution of modes 2 and 3 to } \mathbf{G}(\mathbf{q}, s) \\ &\in \mathbb{R}^{4 \times 1} \end{aligned}$$

$$\begin{aligned} \mathbf{P}_k(\mathbf{q}, s) &= \frac{\mathbf{R}_k(\mathbf{q})}{s^2 + 2\xi_k(\omega_k + \Delta\omega_k)s + (\omega_k + \omega_k)^2} \\ &\triangleq \text{contribution of modes 1 and 4 to } \mathbf{G}(\mathbf{q}, s) \\ &\in \mathbb{R}^{4 \times 1}, \quad k = 1, 4, \end{aligned}$$

$$\mathbf{R}_k(\mathbf{q}) \triangleq \text{the } k^{\text{th}} \text{ mode } \in \mathbb{R}^{4 \times 1}$$

$$\omega_k(\mathbf{q}) \triangleq \text{the } k^{\text{th}} \text{ natural frequency}$$

$$\xi_k(\mathbf{q}) \triangleq \text{the } k^{\text{th}} \text{ damping ratio.}$$

For modes 1 and 4, ξ_k are assumed to be constant and ω_k are assumed to have small variations, $\Delta\omega_k$, due to experimental results which indicate these modes are only weakly configuration dependent. A linear controller is then designed for the system with the linkages at a specific configuration, referred to the design configuration: denoted \mathbf{q}_d . Hence, $\mathbf{P}_k(\mathbf{q}, s)$ for other configurations can be simplified by variable separation within a neighborhood of \mathbf{q}_d , i.e.,

$$\mathbf{P}_k(\mathbf{q}, s) = \mathbf{O}_k(\mathbf{q})\mathbf{H}_k(s) \quad (3)$$

where

$$\mathbf{H}_k(s) \triangleq \mathbf{P}_k(\mathbf{q}_d, s) = \frac{c_k \varphi^{(k)}}{s^2 + 2\xi_k \omega_k s + \omega_k^2} \in \mathbb{R}^{4 \times 1}$$

$$\varphi_k(\mathbf{q}) \triangleq \text{normalized mode shape for the } k^{\text{th}} \text{ mode shape}$$

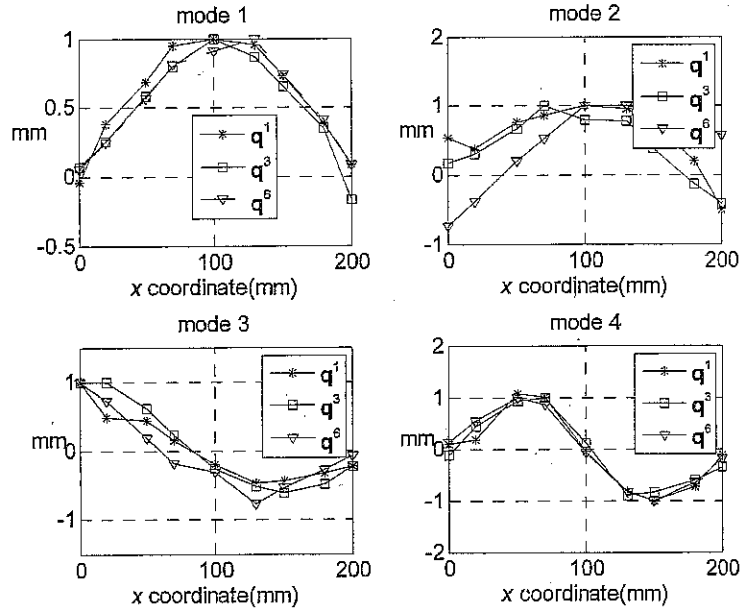


Fig. 7. EMA results during rigid body motion control.

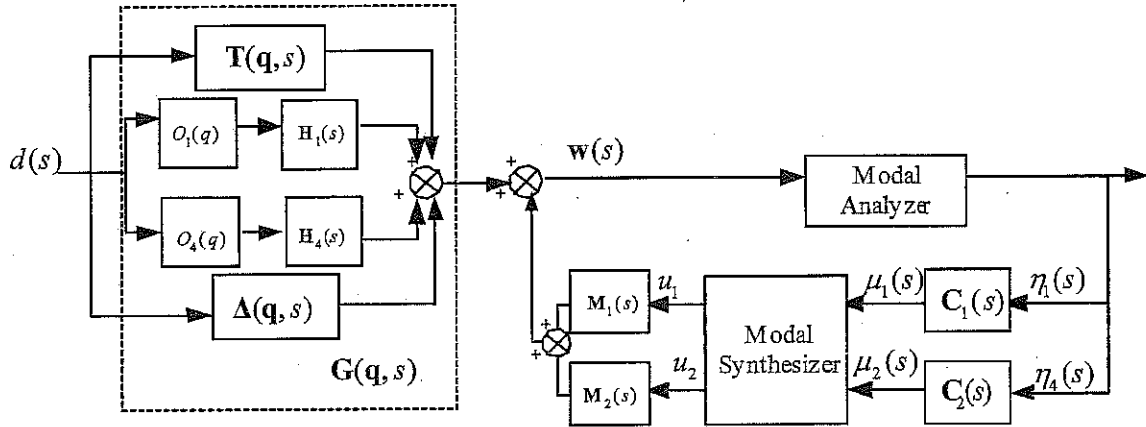


Fig. 8. Simplified transfer function: motor input to linkage vibrations.

$$\in R^{4 \times 1}$$

$c_k \triangleq$ a constant for the k^{th} mode

$$\hat{O}_k(\mathbf{q}) \triangleq \frac{\sum_{i=1}^4 R_{ki}(\mathbf{q})}{\sum_{i=1}^4 R_{ki}(\mathbf{q}_d)}$$

$R_{ki}(\mathbf{q}) \triangleq$ the i^{th} element of $R_k(\mathbf{q})$.

$O_k(\mathbf{q})$ is obtained by making average on different entries of measurements. Hence, the configuration dependency is represented as a combination of configuration-dependent modes, 2, 3, and weakly configuration-dependent modes, 1, 4, as depicted in Fig. 8. The product of $O_k(\mathbf{q})$ and the motor 1 voltage input $d(s)$, $O_k(\mathbf{q})d(s)$, is regarded as the new input to mode 1 and 4. The vibration response of the linkage can then be written as,

$$w(s) = (\mathbf{T}(\mathbf{q}, s) + \Delta(\mathbf{q}, s))d(s) + \mathbf{H}_1(s)(O_1(\mathbf{q})d(s)) + \mathbf{H}_4(s)(O_4(\mathbf{q})d(s)) \quad (4)$$

This simplification forms the basis for the proposed linear active vibration control design. With this approach, $\mathbf{H}_k(s)$ is modified to decrease the sensitivity of the linkage dynamics to excitation near ω_1 and ω_4 , hence suppressing vibrations.

E. Variations in Natural Frequencies for Modes 1 and 4

In Section IV-D, variations of ω_1 and ω_4 are neglected because $\mathbf{H}(s)$ exhibits weak configuration-dependence. However, the small variation of ω_k must be evaluated and considered in the control design, providing the controller with robust performance with respect to changes in natural frequencies. Since the open-loop damping ratios are small and do not change significantly with configuration, the uncertainty in damping ratio is neglected.

$\mathbf{H}_k(s)$ in (2) with uncertainty of natural frequencies $\Delta\omega_k$ can be written as

$$\mathbf{H}_k(s) = \sum_{k=1,4} \frac{c_k \varphi_i^{(k)}}{s^2 + 2\xi_k(\omega_k + \Delta\omega_k)s + (\omega_k + \Delta\omega_k)^2} \quad (5)$$

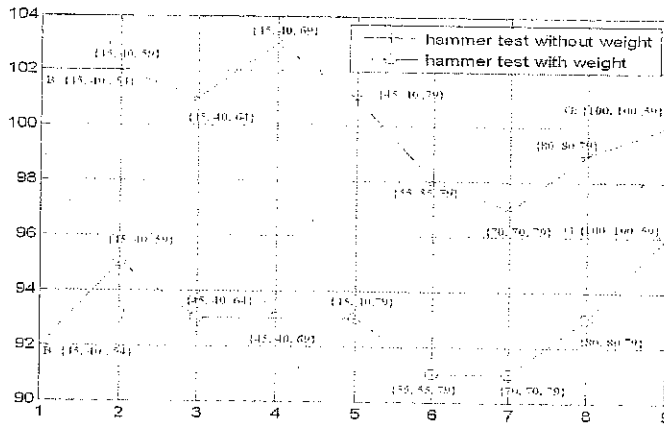


Fig. 9. Change of the first natural frequency along trajectory from configuration B to configuration G .

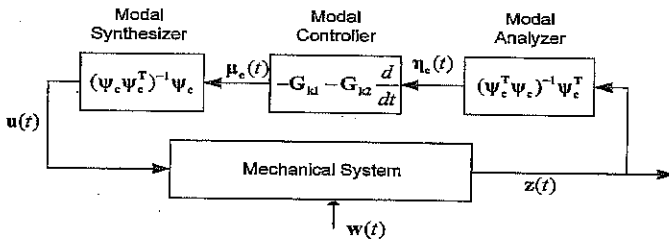


Fig. 10. Schematic of independent modal space control (IMSC).

Experiments are performed to quantify the variation of these natural frequencies. Along a planned trajectory, such as a path from configuration B ($(-52.3, 33.5, 32.6)$ mm) to G ($(-115.3, 34.5, 83.8)$ mm), EMA is performed at nine different configurations, as plotted in Fig. 9 (where configurations are given in the task space, i.e., (x_p, y_p, φ_p)). For the first mode, Fig. 9(a) clearly illustrates the configuration dependent natural frequencies vary only by approximately 6 Hz. Hence, a linear vibration controller is designed in Section V.

In order to examine the robustness of the proposed controller to uncertainties in natural frequencies, a 0.02 kg mass of is attached to the center of the flexible linkage, which is used to provide a perturbation to the natural vibration frequencies. Hammer EMA tests are performed at nine different configurations with the mass attached, with the results plotted in Fig. 9. With this mass added to the flexible linkage, configuration dependent vibration frequencies are observed leading to a decrease in the natural frequencies by up to 10 Hz.

V. VIBRATION CONTROL DESIGN

While the transfer properties from rigid body motion input to linkage vibration have been shown to exhibit configuration dependency, a vibration controller for $H(s)$ is designed in the modal domain based on the assumption that $G(\mathbf{q}, s)$ may be separated into $T(\mathbf{q}, s)$, $O(\mathbf{q})$, and $H(s)$.

A. Active Vibration Controller Architecture

Fig. 10 is a schematic of the active control system, which has four components: plant dynamics, a modal analyzer, a modal domain controller, and a modal synthesizer.

The modal domain governing equation of a linear system with active vibration control can be written as [23]

$$\begin{aligned} \ddot{\eta}(t) + (\text{diag}(2\xi_k\omega_k) + \mathbf{K}_D)\dot{\eta}(t) \\ + (\text{diag}(\omega_k^2) + \mathbf{K}_P)\eta(t) = \psi^T E w(t), \\ k = 1, 2, \dots, N \end{aligned} \quad (6)$$

where

- $\eta(t) \triangleq$ modal coordinates, $\psi(t) \triangleq$ modal matrix
- $\xi_k \triangleq k^{\text{th}}$ damping coefficient, $w(t) \triangleq$ external excitation
- $u(t) \triangleq$ control efforts, i.e., voltages of PZT actuators
- $B \triangleq$ influence matrix for control effort
- $E \triangleq$ influence matrix for external excitation.

As shown in Fig. 10, the modal analyzer is a spatial modal filter $[\psi^T \psi]^{-1} \psi^T$ to estimate modal coordinates $\eta_c(s)$ from the PZT responses. Based on the fact that PZT sensor responses are given by

$$z(t) = \psi \eta(t). \quad (7)$$

Modal coordinates for controlled modes are estimated by multiplying $z(t)$ by the pseudo-inverse of the controlled modes

$$\eta_c(t) = (\psi_c^T \psi_c)^{-1} \psi_c^T z(t) \quad (8)$$

where η_c is modal coordinates for controlled modes, ψ_c is mode shapes for controlled modes.

The modal control algorithm, $C(s) = \{C_1(s) \ C_2(s)\}$, another component of the modal space controller, determines the control output in modal space based on the estimated value of η_c

$$\mu_c(t) = -\mathbf{K}_P \eta_c(t) - \mathbf{K}_D \dot{\eta}_c(t) \quad (9)$$

where

- $\mu_c(t) \triangleq$ modal control effort for the controlled modes
- $\mathbf{K}_P \triangleq$ proportional control gain matrix for controlled modes
- $\mathbf{K}_D \triangleq$ derivative control gain matrix for controlled modes.

$\dot{\eta}_c(t)$ is obtained through time differentiation of $\eta_c(t)$. $\mu_c(t)$ is converted to the physical output to apply to the PZT actuators using the modal synthesizer $\left[\begin{bmatrix} \psi_c \psi_c^T \end{bmatrix}^{-1} \psi_c \right]$, which is the inverse process of the modal analyzer

$$u(t) = [\mathbf{B}^T \mathbf{B}]^{-1} \mathbf{B}^T \left[\begin{bmatrix} \psi_c \psi_c^T \end{bmatrix}^{-1} \psi_c \right] \mu_c(t). \quad (10)$$

Since \mathbf{B} is a square matrix of full rank, $u(t) = \mathbf{B}^{-1} \left[\begin{bmatrix} \psi_c \psi_c^T \end{bmatrix}^{-1} \psi_c \right] \mu_c(t)$. The governing equation in the modal space, with the control algorithm given by, is written as [24]

$$\begin{aligned} \ddot{\eta}(t) + (\text{diag}(2\xi_k\omega_k) + \mathbf{K}_D)\dot{\eta}(t) \\ + (\text{diag}(\omega_k^2) + \mathbf{K}_P)\eta(t) = \psi^T E w(t), \\ k = 1, 2, \dots, N. \end{aligned} \quad (11)$$

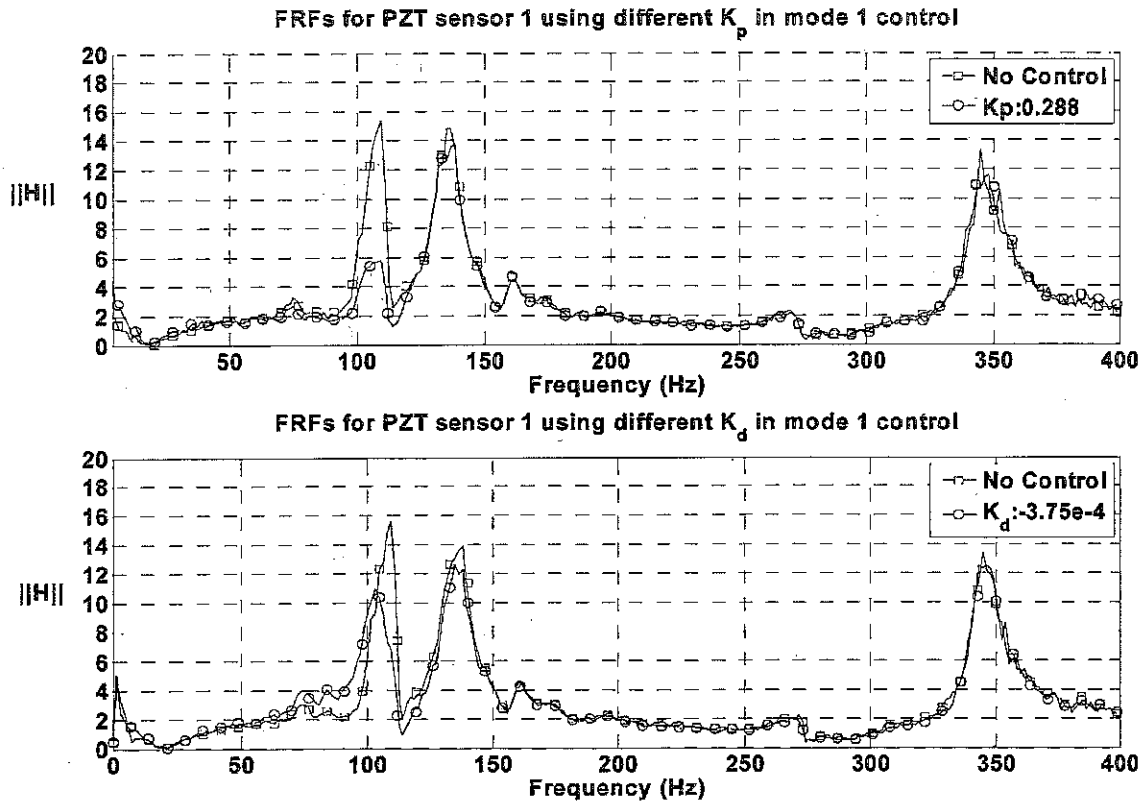


Fig. 11. FRFs from motor 1 to PZT 1: when different K_{P1} and K_{D1} are used in mode 1 control design at configuration *B*.

For the k th mode, the characteristic equation becomes

$$-\omega^2 + (2\xi_k\omega_k + K_{Dk})j\omega + (\omega_k^2 + K_{Pk}) = 0. \quad (12)$$

If the desired natural frequency is ω_{kd} and the desired damping ratio is ξ_{kd} , the gains can be determined

$$K_{Pk} = \omega_{kd}^2 - \omega_k^2, \quad K_{Dk} = 2\xi_{kd}\omega_{kd}^2 - 2\xi_k\omega_k^2. \quad (13)$$

B. Vibration Control Experiments at Configuration *B*

As indicated in Section IV-E, the linkage frequency varies by approximately 6 Hz along the trajectory *BG*, hence a linear vibration controller is designed. For a motion trajectory that exhibits more significant configuration dependency, the approach adopted here can be used by partitioning the robot trajectory into multiple segments, with a controller designed using (13). We evaluate the robustness of this design approach to model uncertainty. Tests are conducted with a small mass attached to perturb natural frequencies.

The vibration controller is designed for mode 1 and mode 4 sequentially because of the decoupled behavior of these modes. Strain based modes, obtained at configuration *B*, are used to construct the modal analyzer using: $\{0.74 \ 0.48 \ 0.38 \ 0.28\}$ for mode 1 and $\{0.86 \ 0.3 \ -0.21 \ -0.36\}$ for mode 4. FRFs are measured when the vibration controller is active to evaluate the effects of vibration controller. Each FRF is measured by averaging ten tests, to improve the estimation accuracy.

Fig. 11 gives frequency-response amplitude plots from the random input of motor 1 to PZT sensor 1, when the only first

mode is controlled. When mode 1 is controlled, other modes are virtually unchanged, confirming the assumption that modes 1 and 4 are decoupled and a good estimate of modal vectors. The first subplot shows results in which different K_{P1} values are used with $K_{D1} = 0$, giving a vibration reduction of 62% in mode 1. The second subplot shows test results in which different K_{D1} values are used and $K_{P1} = 0$ giving a vibration reduction of 30% in mode 1. Based on experimental trial and error to determine gain values, the maximum damping ratio at configuration *B* is achieved with K_{P1} and K_{D1} as 0.24 and -4.13×10^{-4} , respectively.

In Fig. 12, amplitude plots of FRFs from the motor input to four PZT sensors, using the control gains determined for modes 1 and 4, are compared with the FRFs for the case without vibration control. It is observed that vibration amplitudes of mode 1 and mode 4 are substantially reduced with the first natural frequency slightly decreased. The fourth natural frequency has increased by about 10 Hz. Vibration amplitudes for modes 2 and 3 are negligibly changed. It is also noted that the response from the PZT sensors at a lower frequency range is slightly increased. The sum of the peak values of the four FRFs at mode 1 is reduced by 57.5%. The sum of the peak values at mode 4 is reduced by 55.1%.

C. Vibration Control Test With Natural Frequency Uncertainty

Two types of experiments have been carried out to verify the performance of the controller when the natural frequencies are perturbed. In the first test used a 0.02 kg mass is again added to the center of the linkage. The vibration controller, designed at configuration *B* with this mass is then tested. Fig. 13 shows

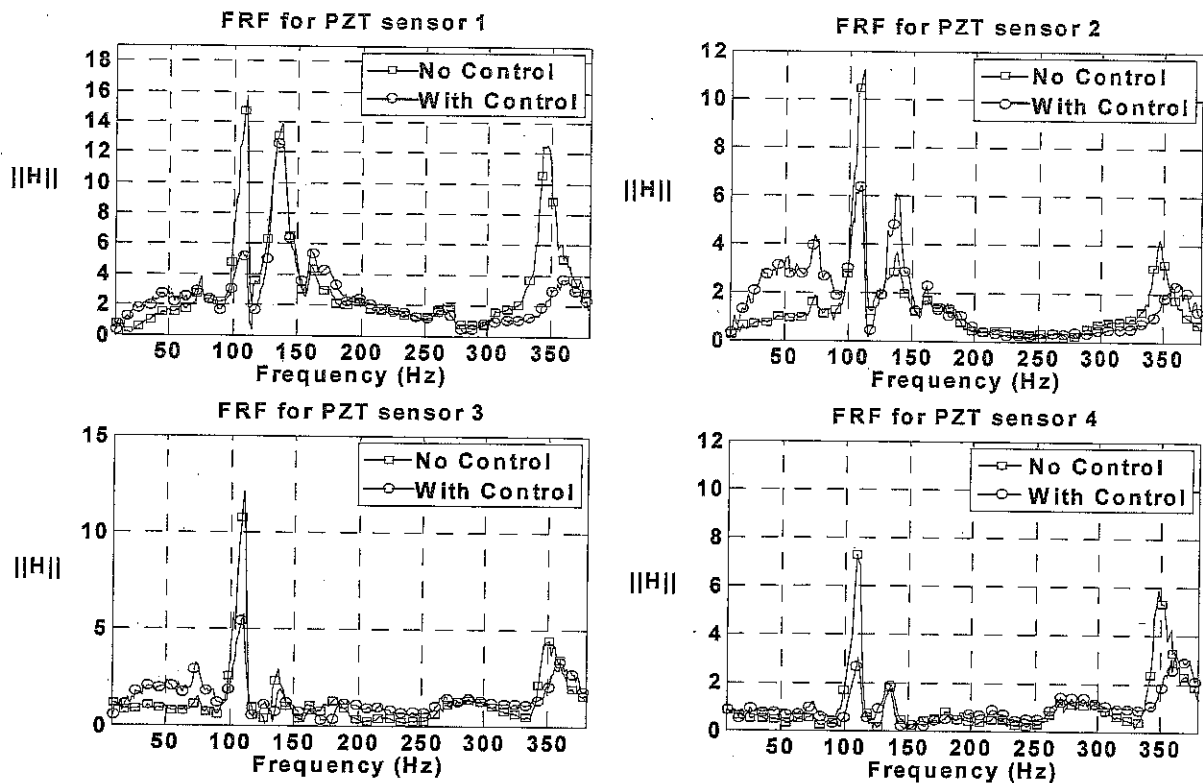


Fig. 12. FRFs from motor 1 to PZT sensor 1: when both modes 1 and 4 are controlled.

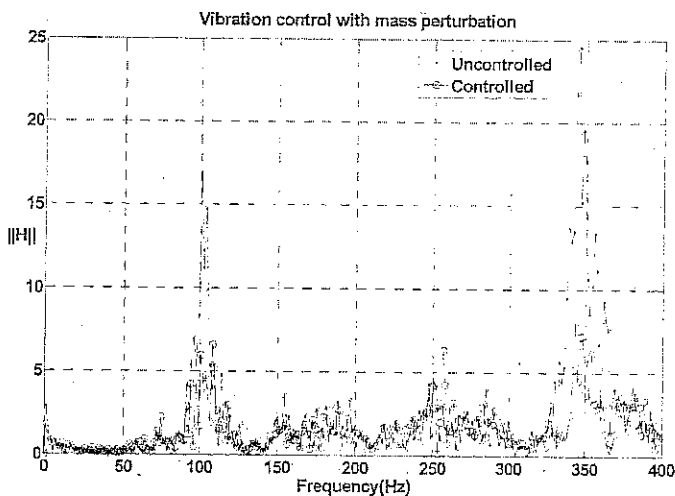


Fig. 13. FRF from motor 1 to PZT sensor 1 with added mass: with and without active vibration control.

the FRF from motor 1 to PZT sensor 1, with active controller on and off. It is demonstrated that proposed vibration controller is effective in damping unwanted structural vibration under uncertain linkage dynamic properties.

Further tests are performed to test the robustness of the controller to configuration dependent vibration frequencies. The vibration controller, designed using the vibration frequencies found at configuration *B*, is tested at configurations *F* ((80.25, 34.2, -40.69) mm) and *G*, with results plotted in Fig. 14. The vibration controller is effective in reducing the unwanted vibration, validating the use of linear controllers.

D. Vibration Control Experiments During Large Amplitude Rigid-Body Motion

In order to further verify the effectiveness of the proposed modal controller during rigid body motion, experiments are performed when the robot undergoes a large amplitude motion from configuration *G* ((-115.35, 34.46, 83.80) mm), to *B*, where the platform comes to rest with residual vibrations. A vibration controller is designed for the parameters determined at configuration *B*. The response spectrums of PZT sensors 1 and 2 are displayed in Fig. 15. The response spectrums of PZT sensors 3 and 4 are also reduced substantially. The sum of the amplitude peaks at mode 1 of four spectrums for PZT sensors is reduced by 50.3%. The sum of the amplitude peaks of four PZT spectrums at mode 4 is reduced by 25%. Note that these amplitudes are already at a very low level, hence a large portion of this signal is attributed to measurement noise.

We compare the proposed controller with a strain rate feedback control [25], with results shown in Fig. 16. In the strain rate feedback control case, average strain rates (i.e., time derivative of sensors) of PZT sensors 1 and 2 are used as feedback to actuator 1 and average strain rates of PZT sensors 3 and 4 is used as feedback to PZT actuator 2. From these plots, it is seen that modal control has superior performance.

VI. CONCLUSION

In this paper, it is experimentally shown that a planar parallel robot exhibits configuration-dependent linkage vibrations. This is caused by nonlinear coupling of rigid-body motion with linkage vibrations and the closed-loop kinematic structure. Using EMA to evaluate FRFs, configuration dependence of

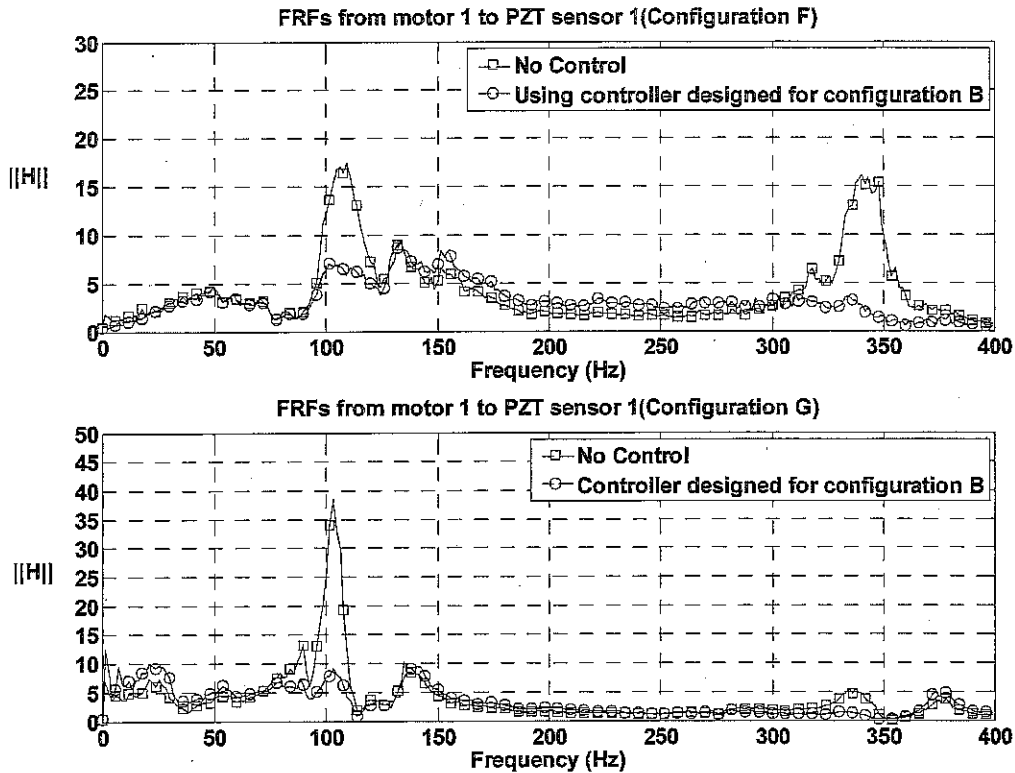


Fig. 14. Vibration controller designed at configuration B used in configuration F and G.

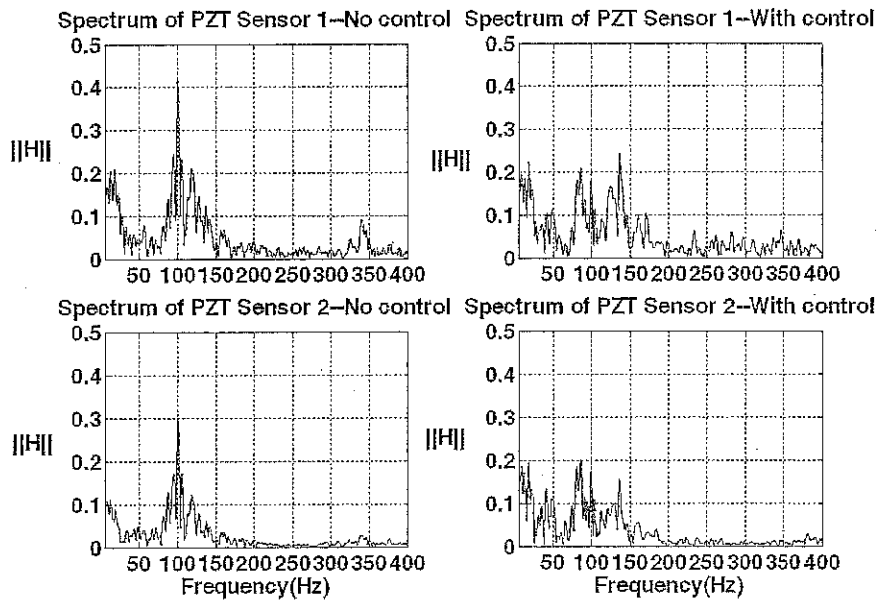


Fig. 15. Comparison of PZT 1 and 2 response spectrums for the case with and without vibration control, during motion from configuration G to configuration B.

linkage mode shapes is determined to be insignificant. Based on this observation, the transfer function from motor voltage input to linkage vibrations is simplified. The contributions of linkage modes are separated from the transfer function. By redefining inputs to linkage modes, the linkage dynamics is assumed to be linear with variations in natural frequencies.

This simplification allows the design of a modal controller based on dynamic parameters obtained for specific robot configuration, providing the configuration dependent natural frequencies do not change with configuration dramatically. Targeting

two linkage modes, vibration controllers are designed to improve structural damping. Experimental evaluation of the proposed control approach verifies that the proposed control exhibits robustness to changes in linkage natural vibration frequency. When the robot undergoes a large rigid-body motion, linkage vibration is suppressed by more than 50%.

This work represents one possible design of a linkage vibration controller for a flexible robotic system exhibiting configuration-dependent vibrations. EMA reveals vibration modes with configuration-dependent FRFs. Providing modal shapes

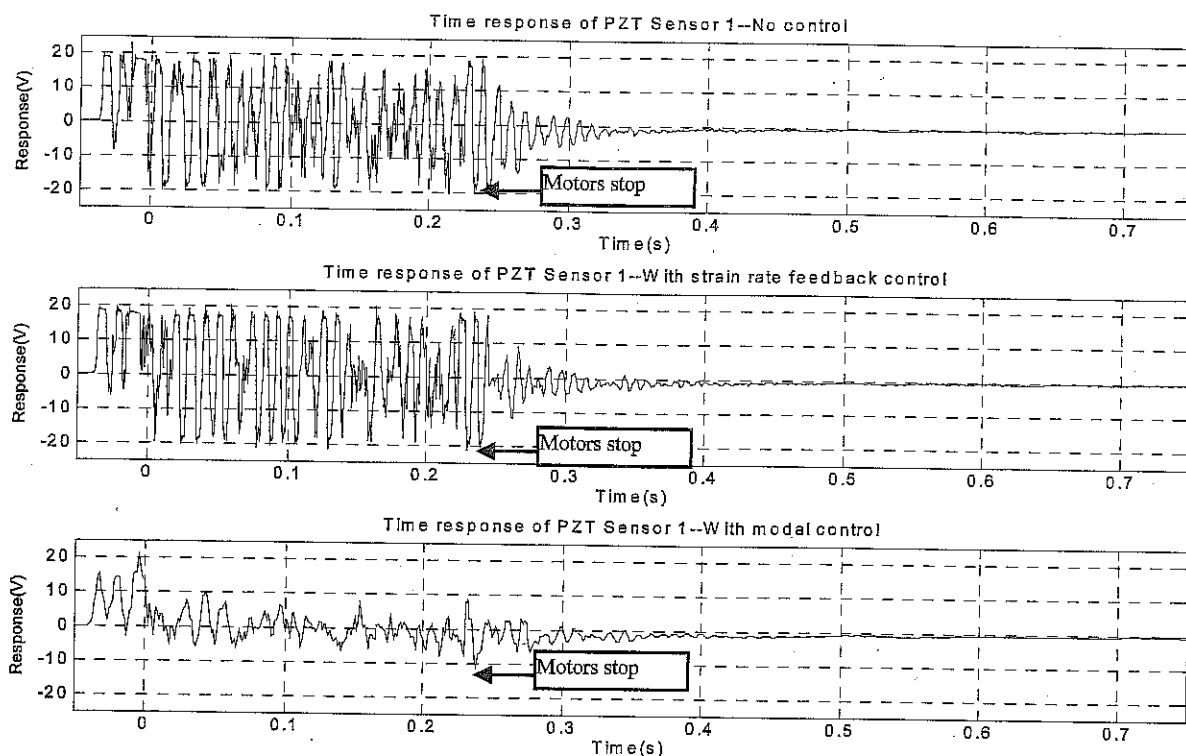


Fig. 16. Comparison of PZT 3 time-domain response for the case of no vibration control, with strain rate feedback, and modal control.

and natural frequencies do not change significantly within certain regions of the robot workspace, the proposed control approach is demonstrated to suppress structural vibration effectively.

REFERENCES

- [1] W. L. Cleghorn, F. G. Fenton, and B. Tabarrok, "Optimal design of high-speed flexible mechanisms," *Mechanism Mach. Theory*, vol. 16, no. 4, pp. 339-406, 1981.
- [2] A. Ghazavi and F. Gardanine, "Dynamic analysis of a composite material flexible robot arm," *Comput. Structure*, vol. 49, no. 2, pp. 315-325, 1981.
- [3] R. L. Clark, W. R. Saunders, and G. P. Gibbs, *Adaptive Structure: Dynamics and Control*. New York: Wiley, 1998.
- [4] E. H. E. H. El-Dammah and S. H. Farghaly, "Vibratory response of a sandwich link in a high-speed mechanism," *Mechanism Mach. Theory*, vol. 28, no. 3, pp. 447-457, 1981.
- [5] J. P. Merlet, *Parallel Robots*. Norwell, MA: Kluwer, 2000.
- [6] I. Heerah, B. Benhabib, B. Kang, and J. K. Mills, "Architecture selection and singularity analysis of a three degree-of-freedom planar parallel manipulator," *J. Intell. Robot. Syst.: Theory Appl.*, vol. 37, no. 4, pp. 355-374, 2003.
- [7] X. Wang and J. K. Mills, "Dynamic modeling of a flexible-link planar parallel platform using a substructuring approach," *J. Mechanisms Mach. Theory*, vol. 41, no. 6, pp. 671-687, 2006.
- [8] C. K. Sung and Y. C. Chen, "Vibration control of the elastodynamics response of high-speed flexible linkage mechanisms," *ASME J. Vib. Acoust.*, vol. 113, pp. 14-21, 1991.
- [9] C. Y. Liao, C. Y., and C. K. Sung, "An elastodynamic analysis and control of flexible linkages using piezoceramic sensors and actuators," *ASME J. Mechan. Des.*, vol. 115, pp. 658-665, 1993.
- [10] S. B. Choi, C. C. Cheong, B. S. Thompson, and M. V. Gandhi, "Vibration control of flexible linkage mechanisms using piezoelectric films," *Mechanism Mach. Theory*, vol. 29, no. 4, pp. 535-546, 1994.
- [11] S. Yuan, Q. Xu, and L. Zhang, "Experiments on active vibration control of a flexible four-bar linkage mechanism," *ASME J. Vib. Acoust.*, vol. 122, pp. 82-85, 2002.
- [12] X. Zhang, C. Shao, and A. G. Erdman, "Active vibration controller design and comparison study of flexible linkage mechanism systems," *Mechanism Mach. Theory*, vol. 37, no. 9, pp. 985-997, 2002.
- [13] H. K. Kim, S. B. Choi, and B. S. Thompson, "Compliant control of a two-link flexible manipulator featuring piezoelectric actuators," *Mechanism Mach. Theory*, vol. 36, no. 3, pp. 411-424, 2001.
- [14] D. J. Ewins, *Modal Testing: Theory, Practice and Application*. Baldock, U.K.: Research Studies Press, 2000.
- [15] W. R. Saunders, D. G. Cole, and H. H. Robertshaw, "Experiments in piezostucture modal analysis for MIMO feedback control," *Smart Mater. Structures*, no. 3, pp. 210-218, 1994.
- [16] B. T. Wang and C. C. Wang, "Feasibility analysis of using piezoceramic transducers for cantilever beam modal testing," *Smart Mater. Structures*, no. 6, pp. 106-116, 1997.
- [17] A. Midha, D. Karam, D., and B. S. Thompson, "Elastic slider-crank mechanism. A study of the intrinsic configuration-dependent modal properties," in *Proc. 22nd Biennial Mechanisms Conf.*, 1992, pp. 337-346.
- [18] A. A. Shabana, "Flexible multibody dynamics: Review of past and recent developments," *J. Multibody Syst. Dyn.*, vol. 1, no. 2, pp. 189-222, 1997.
- [19] D. S. Hardage and G. J. Wiens, "Modal analysis and modeling of a parallel kinematic machine," in *IMECE Proc. ASME: Manufacturing Sci. Eng.*, Nashville, TN, MED- Nov. 14-19, 1999, vol. 10, pp. 857-862.
- [20] X. Wang and J. K. Mills, "Experimental identification of configuration dependent linkage vibration in a parallel robot using smart material actuators and sensors," *Trans. Canadian Soc. for Mech. Eng.*, vol. 31, no. 1, pp. 57-73, 2007.
- [21] X. Wang and J. K. Mills, "Modal control design of configuration-dependent linkage vibration in a parallel robot through experimental identification," in *Proc. IEEE/RSJ Int. Conf. Intell. Robots Syst.*, Beijing, China, Oct. 2006, pp. 3225-3230.
- [22] X. Wang and J. K. Mills, "FEM dynamic model for active vibration control of flexible linkages and its application to a planar parallel manipulator," *J. Appl. Acoust.*, vol. 66, no. 10, pp. 1151-1161, 2005.
- [23] L. Meirovitch, *Dynamics and Control of Structures*. New York: Wiley Interscience, 1990.
- [24] D. R. Morgan, "An adaptive modal-based active vibration control system," *J. Acoust. Soc. Amer.*, vol. 89, no. 1, pp. 248-256, 1991.
- [25] G. Song, S. P. Schmidt, and B. N. Agrawal, "Experimental study of active vibration suppression of flexible structure using modular control patch," in *Proc. IEEE Aerosp. Appl. Conf.*, Los Alamitos, CA, 1998, vol. 1, pp. 189-201.